https://doi.org/10.25686/7230.2020.6.58828

ASSESSMENT OF LAND SURFACE TEMPERATURE AND DROUGHT INDICES FOR THE KLERKSDORP-ORKNEY-STILFONTEIN-HARTEBEESFONTEIN (KOSH) REGION

Noluvuyo Dudumashe, Abraham Thomas
Council for Geoscience, Pretoria 0184, South Africa.

Land surface temperature (LST) is a key calculator of local climate, vegetation growth, and urban change. Spatial and temporal variation of LST over land use/land cover (LULC) features results in changes in environmental factors that influence the characteristics of the land surface. In this study, some remote sensing techniques have been applied to Landsat 8 data acquired during summer and spring seasons of years 2019, 2018, and 2013 to estimate normalized difference vegetation index (NDVI), LST, normalized difference built-up index (NDBI), three drought indices viz. vegetation supply water index (VWSI), crop water supply index (CWSI) and temperature condition index (TCI) and analysed the spatial-temporal trends in LST among major LULC of an arid part of North West Province of South Africa known as Klerksdorp-Orkney-Stilfontein-Hartebeesfontein (KOSH) region. The results shows that there is a direct negative relationship between LST and NDVI. The study compared three drought indices for monitoring the water scarcity of the area. The finding also indicates a positive relationship between LST and CWSI that is relevant to soil moisture and NDBI. The findings from the study prove the capability of optical remote sensing in monitoring LST and drought in the region. The study reveals the usefulness of the remotely sensed data of Landsat 8 satellite in estimating LST and drought changes in the KOSH area. This study also tried to assess the usefulness of Landsat 8 bands in deriving vegetation index and drought indices for monitoring drought in the KOSH region during three years (2013, 2018 and 2019).

Keywords: *Landsat 8, land surface temperature, drought, remote sensing, vegetation and drought indices, climate change.*

Introduction

Land surface temperature (LST) is the primary climatic parameter in calculating the surface radiation and the energy exchange (He et al., 2019). Climate change is one of the most critical challenges that the world faces. Many studies have reported that climate change has a significant effect on the land surface temperature and its other parameters (Brohan et al., 2006; Hansen et al., 2010). Simó et al. (2016) stated that LST is also important for controlling the dynamics of the earth's surface. Land use/land cover (LU/LC) and land surface temperature (LST) is the most important amid these parameters. Several researchers used LST for understanding changes in temperature fluctuations which are major aspects that change the land use/land cover (Owojori and Xie, 2005). LST is defined as the temperature felt when there is an exchange of long-wave radiation and turbulent heat fluxes within the surface-atmosphere interface. The LST is being increasingly used to evaluate climate change in urban zones. Several techniques previously have been applied for calculating land surface temperature through ground base data, but that is costly (Rehman et al., 2015). LST is needed for better environmental monitoring and climate change mitigation.

The time-series observations are frequently employed in monitoring approaches related to remote sensing (RS) and LST. The application of time series in the assessment of the climate variability over an extended period can be improved by the integration of spatial data from multiple satellite systems (Kothe et al., 2019). The Landsat imageries are the most valuable source of spatial information at 30-m resolution (Herrero-Huerta et al., 2019). It is also useful in continuous global coverage to provide an opportunity to characterize human-scale processes (Chen et al., 2017). Chastain et al. (2019) stated that operational Landsat 8 (OLI & TIRS) could supply a revisit frequency of 8 days at the equator. The Landsat sensors have a high spatial resolution helping in the monitoring of the urban thermal environment (XIAO et al., 2007a; Sobrino et al., 2012). Thermal infrared (TIR) bands are very important bands in estimating LST in an area and monitoring climate change. The USGS recommendation is not to use TIRS Band 11 due to its larger calibration uncertainty, only Band10 was used in the LST calculation. However, not every remote sensing

platform has the thermal-infrared bands on their sensor.

Ustin et al. (2004) stated that remote sensing must play a part in providing the data required to monitor the conditions and change of ecosystem at all spatial scales. This is an increasing field of environmental scientists. Therefore, acquiring LST from remotely sensed data becomes one of the important main factors for such studies. Torrion et al. (2014) outlined that LST is associated to surface energy fluxes, the latent heat flux, and evapotranspiration and water stress. According to Cammalleri and Vogt (2015), LST is connected to surface longwave emission and calculating soil moisture. Whereas Duan et al. (2014) stated that considering meteorological and hydrological processes in a changing climate is the best parameter in estimating LST. The presented study aimed to estimate the LST using Landsat 8 images acquired during the year 2013, 2018, and 2019, to map and monitor the area for changes in LST and drought through drought monitoring indices viz. vegetation supply water index (VWSI), crop water supply index (CWSI) and temperature condition index (TCI), and to compare the results for these three years.

Study area

The Klerksdorp-Orkney-Stilfontein-Hartebeesfontein (KOSH) region was selected as a study area. The geographic location of the KOSH area is in the North West province of South Africa (fig. 1). The region comprises four districts, namely Klerksdorp, Orkney, Stilfontein, Hartebeesfontein, covering an area of 2757 km^2. The climate of the region is warm to hot summers (November to February/March) and cool, dry winters (May to August) are typical. KOSH region is part of the Witwatersrand gold mining area, underlain by sedimentary, extrusive, and intrusive rocks of Transvaal Super Group (Thomas, 2020). Figure 2 depicts the land use/land cover of the area showing that the most area is covered by the grassland cover.

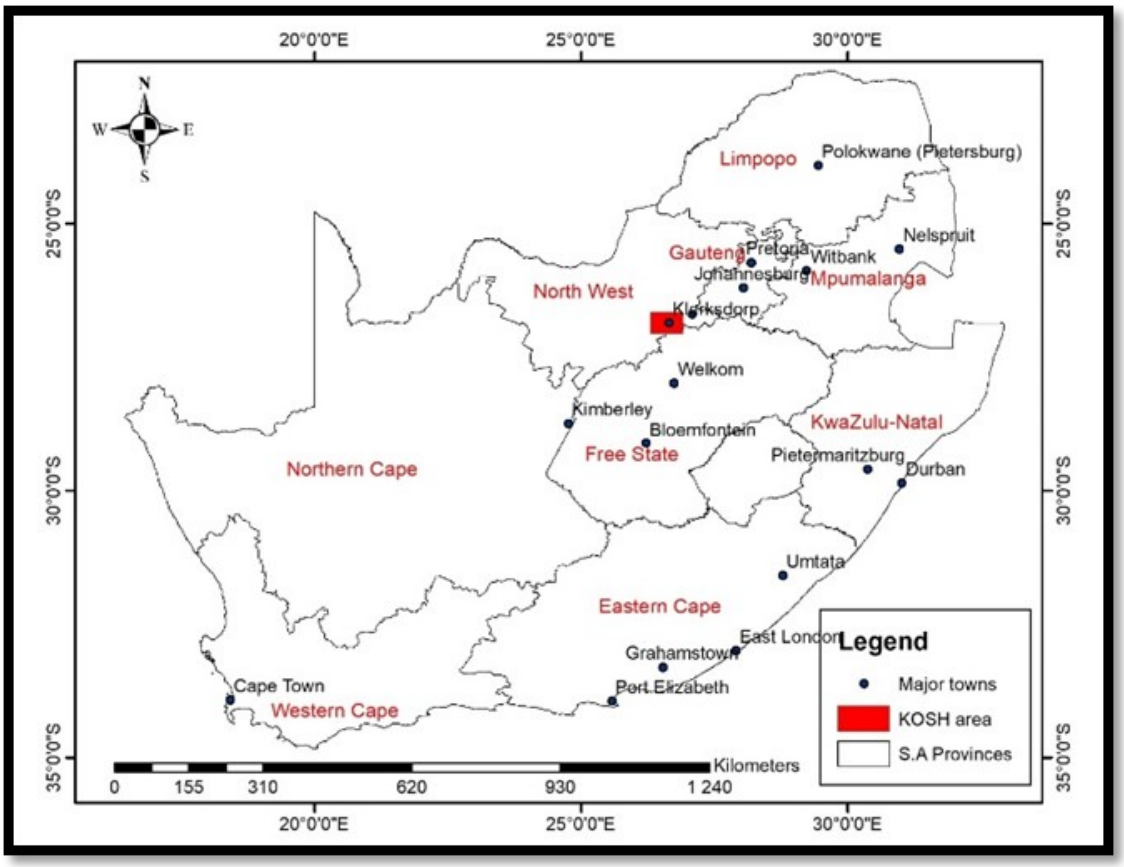

Fig. 1. Location map of Klerksdorp-Orkney-Stilfontein-Hartebeesfontein (KOSH) region

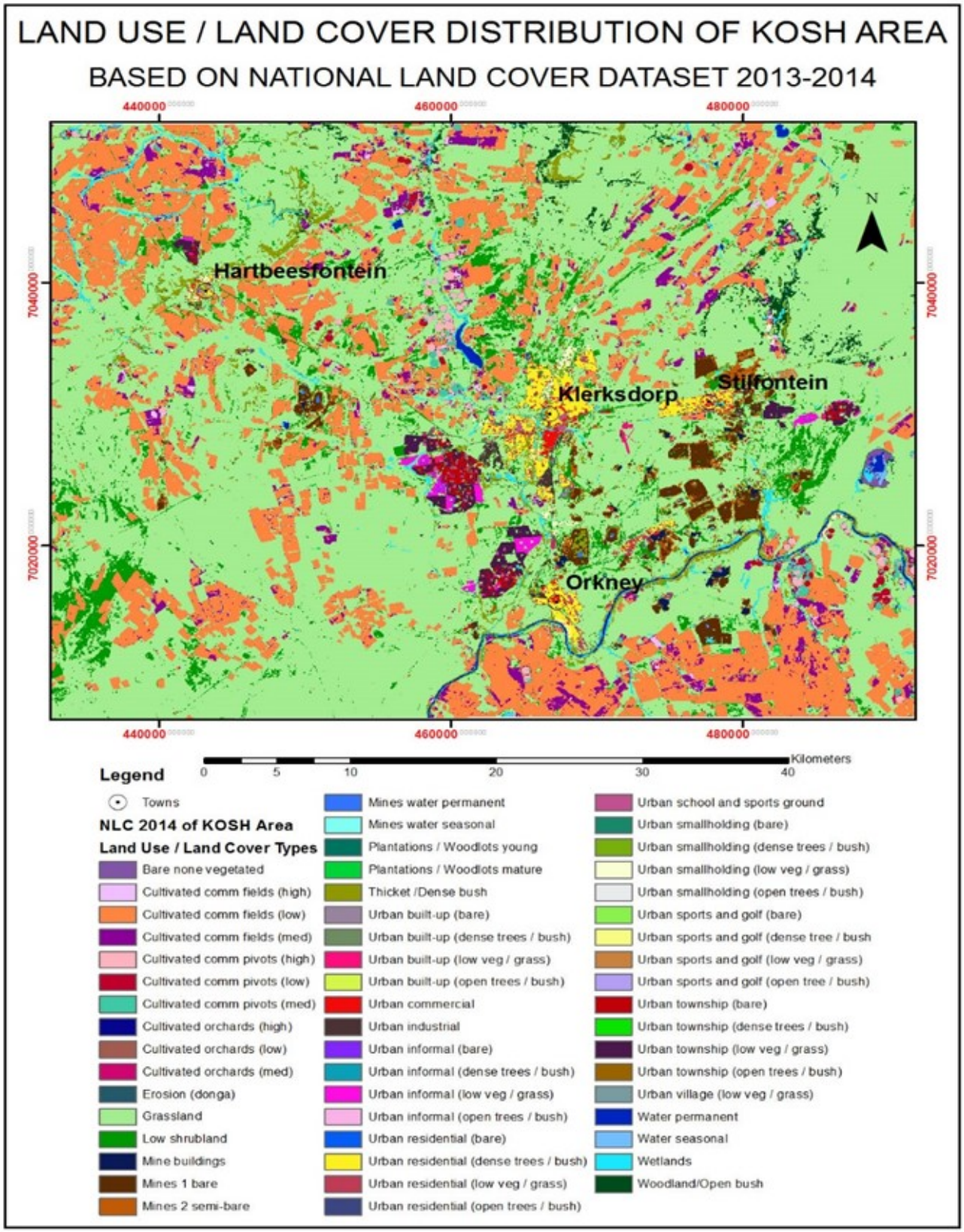

Fig. 2. Land use/ Land cover distribution of Klerksdorp-Orkney-Stilfontein-Hartebeesfontein (KOSH) area based on national land cover dataset 2013-2014

Data and software used for the research

Data used for remote sensing analysis

In this study, the first step was downloading Landsat 8 satellite data (cloud cover of 0%) of KOSH region from the USGS Earth Explorer website (https://www.usgs.gov/). The level-1 prod-

uct Landsat 8 data acquired during summer and spring seasons of three-years (2013, 2018, and 2019) were searched. The images were georeferenced using ArcGIS software to the Universal Transverse Mercator (UTM) Projection System. The images of Landsat 8 (footprint: 171/079) was used in this study. Satellite data were acquired over two different seasons (end of summer and the beginning of spring) for three different years to assess and monitor the study over time. Fig 3 shows the extent of the spatial coverage with the study area and Table 1 shows the band details of the data used. Thermal bands (TIR) were used for the calculation of the land surface temperature (LST) without being pre-processed. The band 10 was used from Landsat 8 OLI due to larger calibration uncertainty of band 11 found to have.

Table 1

Landsat image characteristics used in this research (Source: NASA 2003, USGS 2015)

Characteristics	Landsat 8 OLI/TIRS
Band number	30 m: Band 1- Coastal aerosol Band 2 – Blue Band 3 – Red Band 4 – Green Band 5 – NIR Band 6 – SWIR -1 Band 7 – SWIR -2 Band 9 – Cirrus 15m: Band 8 – Pan 100m: Band 10 - TIR -1 Band 11 – TIR - 2
Thermal band spectral range	Band 10 (10,60 – 11,19 nm) Band 11 (11,50 – 12,51 nm)
Acquisition dates	Summer 26/03/2013 03/02/2018 22/02/2019 Spring 02/09/2013 15/09/2018 02/09/2019

The software used for this study were ArcGIS 10.4 version and ENVI 5.5 version. LST and Normalized satellite indices were calculated using the raster calculator tool of ArcGIS 10.4. The shapefile of respective areas were created and area of interest (AOI) was extracted using ArcGIS.

Methodology

Land surface temperature (LST) calculation is one of the steps to determine the drought on the Earth's surface. The remotely sensed images can be used to derive this information using algorithms that are specifically developed to provide information using 'RT' – Real-time Terrain Corrected dataset containing both OLI & TIRS bands. The three bands used in this study are band 4, band 5 and thermal band 10. The thermal band 10 of this dataset was not processed for atmospheric correction and surface reflectance retrieval for land surface temperature; however, the red and near-infrared bands (bands 4 and 5) were pre-processed using ENVI software for atmospheric correction. Later NDVI values were calculated in ENVI software using the red and near-infrared bands.

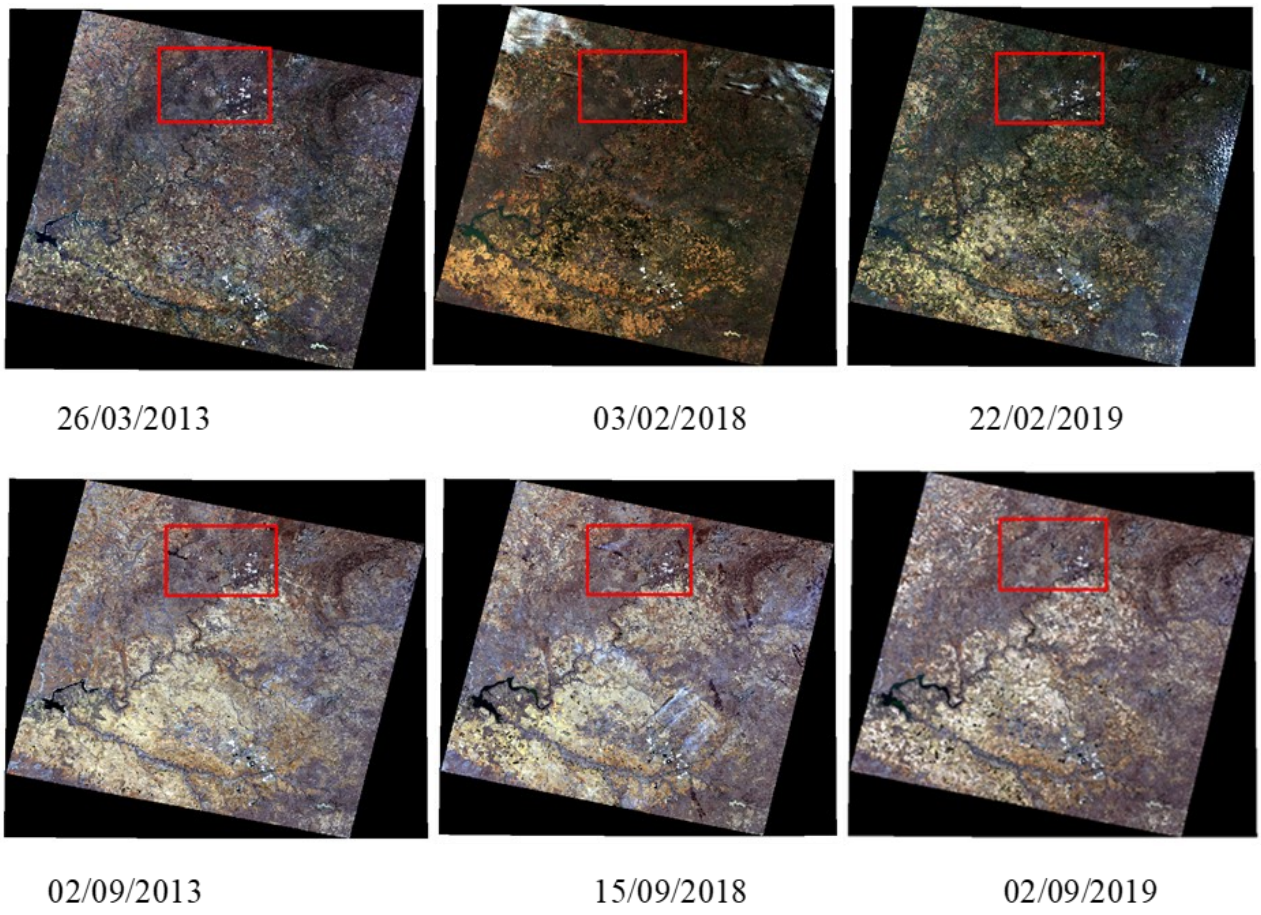

Fig. 3. Preview images of the used data of 2019, 2018, and 2013 to see the extent of spatial coverage with the extent of the study area

Equations used to calculate Land Surface Temperature with Landsat 8 satellite images

TOA (Lλ) spectral transmittance

The first step in computing LST is to transform the DN of the thermal infrared band into spectral radiance (Lλ) by using the following equation obtained from the Landsat user's handbook. The reason for transforming the DN was to calibrate for the produced noise from the sensors, which measure the reflectance from the Earth's surface in the form of Digital Numbers (DN) representing each pixel.

$$L\lambda = ML * Qcal + AL\,, \tag{1}$$

where ML is the band specific multiplicative rescaling factor from the metadata, AL is the band specific additive scaling factor and Qcal represents the symbolized values of quantized and calibrated standard product pixels (D). The DN of Landsat 8 of band 10 images were converted to spectral radiance, using the above equation which is given by Rosas et al. (2017).

Brightness Temperature

The second step is to convert the band radiance into brightness temperatures (TB) in Celsius using a conversion formula given below (equation 2). The TIR data values of band 10 were converted to brightness temperatures (TB), which is the microwave radiance travelling upward from the top of Earth's atmosphere, using the thermal constants provided in the metadata file (Yang et al., 2014). To achieve accuracy for the TB conversion, equation 2 was implemented through the ATCOR module of ArcGIS. The result in Kelvin was converted to Celsius by adding the absolute zero.

$$TB = (K2 / (\ln (K1 / L) + 1)) - 273.15\ , \quad (2)$$

where TB is the satellite brightness temperature in Celsius, and K1 and K2 represent thermal conversion from the metadata (Suresh et al., 2016). Table 2 shows the constants K1 and K2 used for the Landsat satellites.

Table 2

Constants K1 and K2 for the Landsat satellites

Constant	Landsat 8 (Band 10)	Landsat 8 (Band 11)
K1 (watt/meter squared *ster*)	774.89	480.89
K2(Kelvin)	1321.08	1201.14
Rescaling	ML 0.0003342 AL 0.10	

Table 3

Center wavelength for Landsat satellites.

Satellite	Band	Center Wavelength
Landsat (OLI) 8	10	10.8
Landsat (OLI) 8	11	12

Normalized Difference Vegetation Index (NDVI)

NDVI is an indicator used to analyse the greenness of the observed area. As Weng et al. (2004) stated, estimating NDVI is essential since the amount of vegetation present is a factor for LST retrieval. NDVI is calculated using the following equation/formula:

$$NDVI = NIR\,(band\ 5) - Red\,(band\ 4) / NIR\,(band\ 5) + Red\,(band\ 4)\ , \quad (3)$$

where NDVI values range between −1 and 1.

Proportion of Vegetation Cover

Following the NDVI calculation, the vegetation index (Pv) was calculated according to the equation as described by XIAO et al. (2007b). According to Jin et al. (2015) and Quintano et al. (2015), the proportion of vegetation (Pv) is computed by using soil and vegetation NDVI values calculated by Equation 4:

$$Pv = Square\ ((NDVI - NDVImin) / (NDVImax - NDVImin)), \quad (4)$$

where NDVI is the normalized difference vegetation index. $NDVI_{min}$ and $NDVI_{max}$ are the minima and maximum values of the NDVI (Sobrino and Romaguera, 2004).

Estimation of emissivity

The land surface emissivity was derived from the NDVI as proposed by Ngie et al. (2017). According to Pal and Ziaul (2017), the Ground Emissivity (ε) values are calculated using equation 5:

$$\varepsilon = m^* P_v + 0.986\ , \quad (5)$$

where m=0,004 and n=0,986. PV is the proportion of vegetation extracted from equation (4).

Land Surface Temperature

The Land surface temperature (LST) is estimated from the brightness temperature (TB). For estimating brightness temperatures (TB), it is assumed that the Earth is a blackbody, which is not, and this assumption can lead to some errors in surface temperature (Ogunode and Akombelwa, 2017). To minimize these errors, emissivity correction is important and this correction applied to equation 2 to retrieve the LST from TB:

$$LST = (TB / (1 + (0.00115 * TB / 1.4388) * Ln(\varepsilon))) . \quad (6)$$

The main data processing steps (workflow) to be followed for data analysis using a GIS or a remote sensing software for retrieving LST from the Landsat 8 data is shown in figure 4.

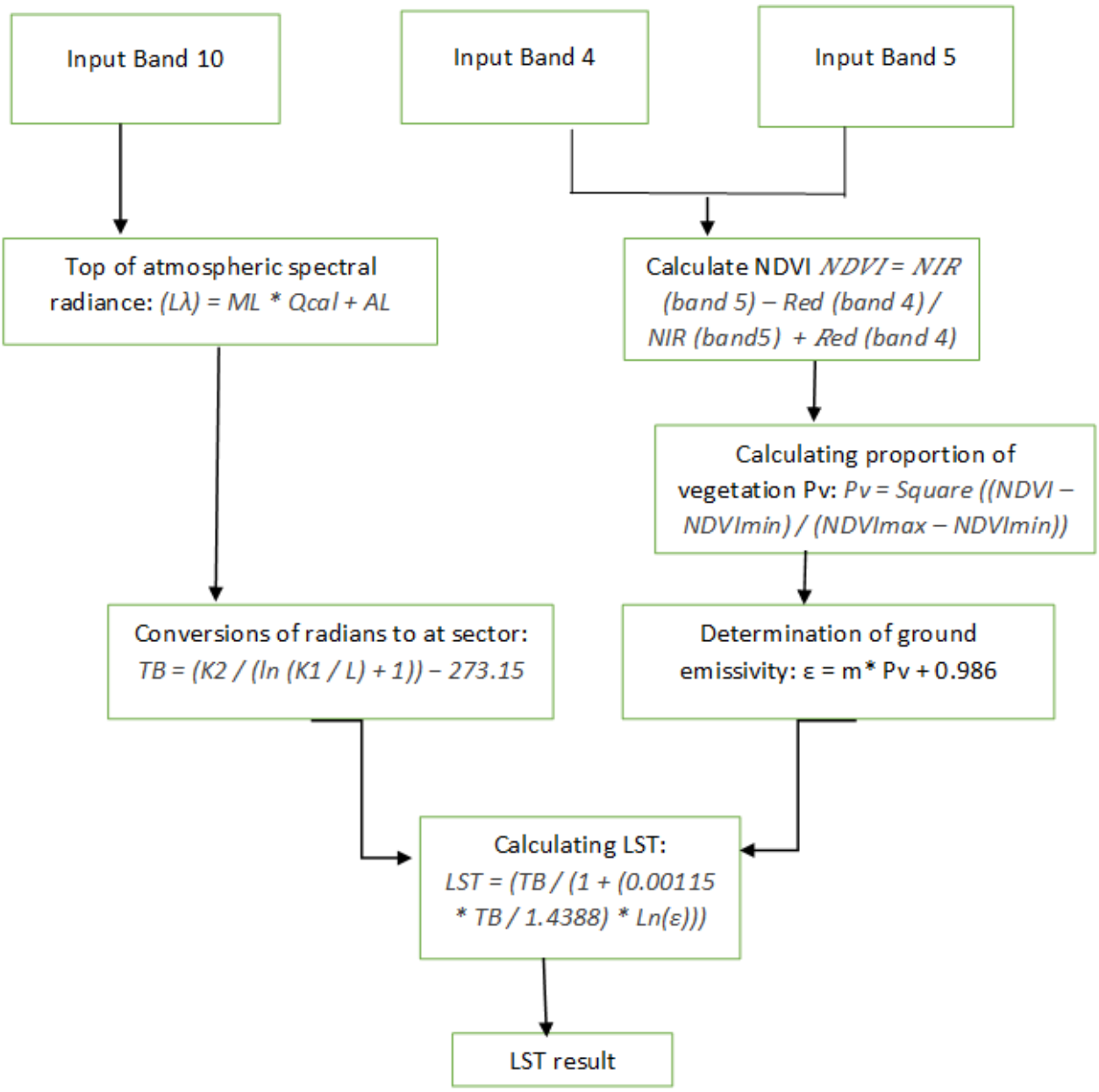

Fig. 4. LST retrieval flowchart

Normalized Difference Built-up Index

The NDBI is an index which is used to detect built-up area from other LULC types. The value of the NDBI is between -1 and 1, where the negative values indicate water body and positive value represent areas that have higher built up and other paved surface areas; whereas zero NDBI values represent areas covered with vegetation (Balew and Korme, 2020). This index can be computed as:

$$NDBI = B_{SWIR} – B_{NIR}/B_{SWIR} + B_{NIR} , \quad (7)$$

where B_{SWIR} is shortwave infrared band reflectance (band 6 of Landsat 8).

Drought indices: temperature condition index (TCI), crop water stress index (CWSI) and vegetation water supply index (VSWI)

Three drought indices were computed in this study to compare the drought in three different years. The first drought indices were calculated using the Temperature Condition Index (TCI) algorithm. Temperature Condition Index (TCI) is an algorithm developed by Kogan (1998) for detecting drought by viewing the difference from the surface temperatures level resulting in water-saturated soil, which affects vegetation stress level (Equation 8).

Secondly, we calculated the drought using the crop water stress index (CWSI) to identify areas where the crops are under water stress. Crop Water Stress Index (CWSI) is a technique for detecting drought due to water lost through evapotranspiration (Equation 9). Lastly, the vegetation supply water index (VSWI) calculated by dividing NDVI values with LST values (equation 10) was also used in identifying areas with drought. The three drought indices have an opposite index value explanation; zero in TCI indicates drought condition, but the wet condition in CWSI. The last index vegetation water supply index was used. Vegetation supply water index is the water supply in the vegetation. The reason for using the three indices was to compare the drought results and see if the algorithm can identify the same area with drought.

$$TCI = (LSTmax\text{-}LST/LSTmax\text{-}LSTmin)*100 , \quad (8)$$

$$CWSI = LST\text{-}LSTmin/LSTmax\text{-}LSTmin , \quad (9)$$

$$VSWI= NDVI/LST . \quad (10)$$

Statistical analysis is very important to analyse different variables. In this study, descriptive statistical analysis was applied for analysing LST, NDVI and NDBI for each study period. The results from this statistical analysis mainly show the mean, minimum, maximum and standard deviation of the calculated indices for different periods of study.

Results and discussion

The spatial-temporal pattern of Normalised difference vegetation index

Figure 5 and figure 6 show the spatial distribution/variation of NDVI values for the summer/spring periods of the year 2013, 2018 and 2019. The most affected areas are in the northern, middle, western and central parts of KOSH. Particularly the middle region of the KOSH shows an extreme drought condition. Results presented in figure 5 (summer 2013, 2018 and 2019), indicate that NDVI values observed were ranged from −0.27 to 0.64. Most areas of the KOSH had low NDVI because of low vegetation cover and high vegetation in areas with vegetation. However, places seen to the east of KOSH had lower NDVI values because the area's lack of vegetation cover and bare surfaces dominate the area 2018. In 2013, the maximum NDVI value was 0.57 and a minimum of -0.33 and with a mean of 0.17. However, the minimum, maximum and mean NDVI values in 2018 were increased to -0.27, 0.64, and 0.25. Furthermore, in the year 2019, the maximum NDVI was 0.63 but in the spring of 2019, it was declined to 0.59 (fig 6), while the mean decreased from 0.08 to 0.04 (table 4).

Table 4

Statistical summary of NDVI values in KOSH (2013, 2018 and 2019).

Year	Mean	Max	Min	STD
2013 Summer	0.17	0.57	-0.33	0.04
2013 Spring	0.11	0.56	-0.41	0.03
2018 Summer	0.25	0.64	-0.27	0.07
2018 Spring	0.13	0.60	-0.30	0.03
2019 Summer	0.29	0.63	-0.29	0.08
2019 Spring	0.14	0.59	-0.32	0.04

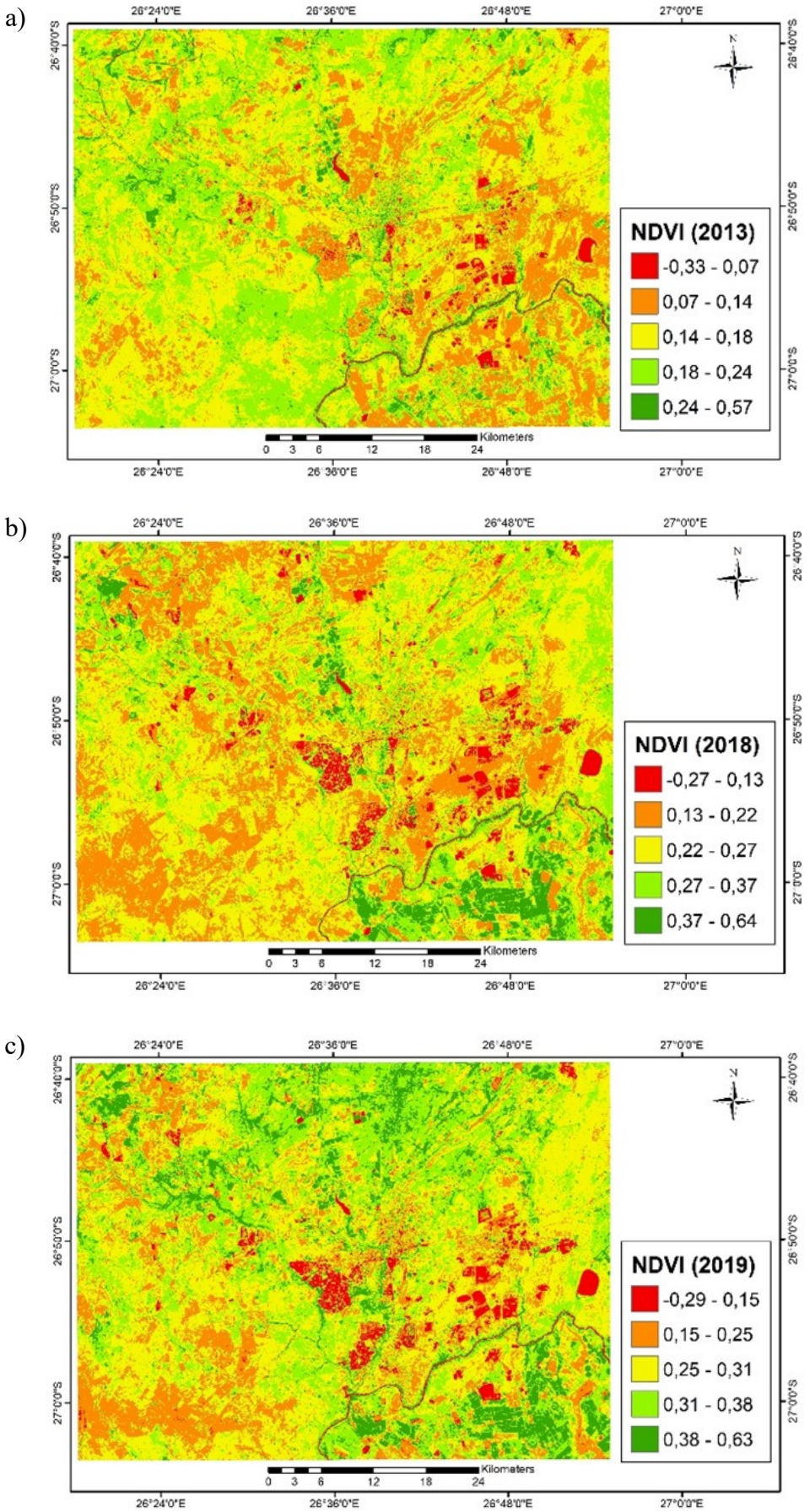

Fig. 5. Spatial-temporal pattern of NDVI dynamics of KOSH during the summer seasons of the year (a) 2013, (b) 2018, and (c) 2019

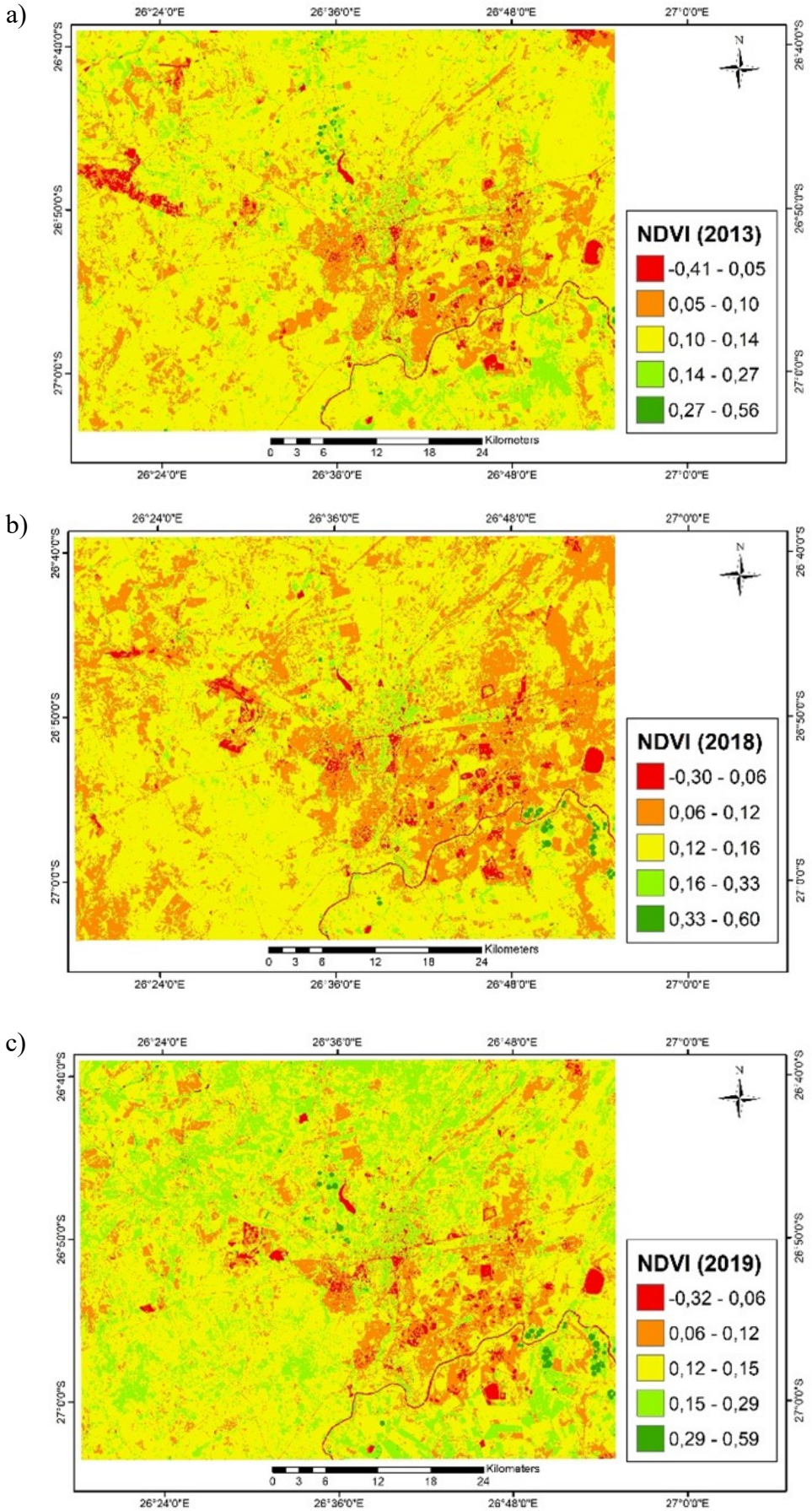

Fig. 6. Spatial-temporal pattern of NDVI dynamics of KOSH during the spring season of the year (a) 2013, (b) 2018 and (c) 2019

The spatial-temporal pattern of Land Surface Temperature

Figure 7 and figure 8 shows the spatial pattern results of LST and Table 5 shows statistical information. The green colour indicates that the areas have very low temperatures with certain land cover such as; the body of water, woodlands and area of shadows, or clouds (fig. 7 and fig. 8). On the three images selected in summer the north-west, south-west, northeast and east-south parts experienced higher LST ranging from 25.09 – 36.83 and in the areas with lower LST it ranges from 15.44 – 26.25. However, in some grassland areas, the LST ranges from 22.54 to 29.56. In spring results, 2013 and 2019 the maps show close similarity results than the results of 2018. LST value is high in most of the area because the area is mostly covered by short grass. In the spring season, high values are seen because the grass is very short and dry. The south-east part of the area is covered with water (river) and vegetation (crops/woodlands) so those areas have low LST and high NDVI values. The western and southwest part with grassland show high values of LST. NDVI has a negative correlation with LST meaning that the higher the NDVI the lower the LST. Similarly. In areas of the higher LST values, one can find lower NDVI values. There is a decrease in the values of statistical parameters between the season in all three years because of the difference in the climate of these seasons. The finding proves that where the region has high vegetation cover, the land surface temperature is less in such regions and where there is lesser vegetation cover, then the land surface temperature is higher.

Table 5

Statistical summary of LST (℃) values in KOSH and its surrounding (2013, 2018 and 2019)

Year	Mean	Max	Min	STD
2013 Summer	23.35	34.23	15.44	1.32
2013 Spring	22.44	34.07	9.14	1.97
2018 Summer	37.61	48.39	18.80	1.22
2018 Spring	34.72	94.97	18.37	2.53
2019 Summer	28.90	35.91	21.06	1.49
2019 Spring	27.73	41.35	15.44	1.95

The spatial-temporal pattern of Normalised Difference Built Index (NDBI)

Results indicate that during the year 2013 summer, the Normalised Difference Built Index (NDBI) values ranged from − 0.45 to 0.27 with the lowest temperature and highest temperature of 0 and 100 °C (fig. 9). In the year 2018, summer the NDBI values ranged from − 0.54 to 0.33 with the lowest temperature and highest temperature being 0 and 100 °C respectively (fig. 9). Whereas in the year 2019 the NDBI values ranged from -0.49 to 0.26. However, for the spring season in 2013, the range of NDBI is from -0.46 to 0.30, in the year 2018 it is between -0.46 to 0.73, and in the year 2019, it ranged between -0.48 to 0.27 (fig. 10). NDBI has a positive correction with LST that is the lower the NDBI the lower the LST and the higher the NDBI indicate higher the LST. In the study, there was a positive relationship between NDBI and LST. According to Faris and Reddy (2010), Built-up land plays the biggest role in increasing the temperature because of the hard concrete surface which contains almost nil water storage which leads to less humidity also.

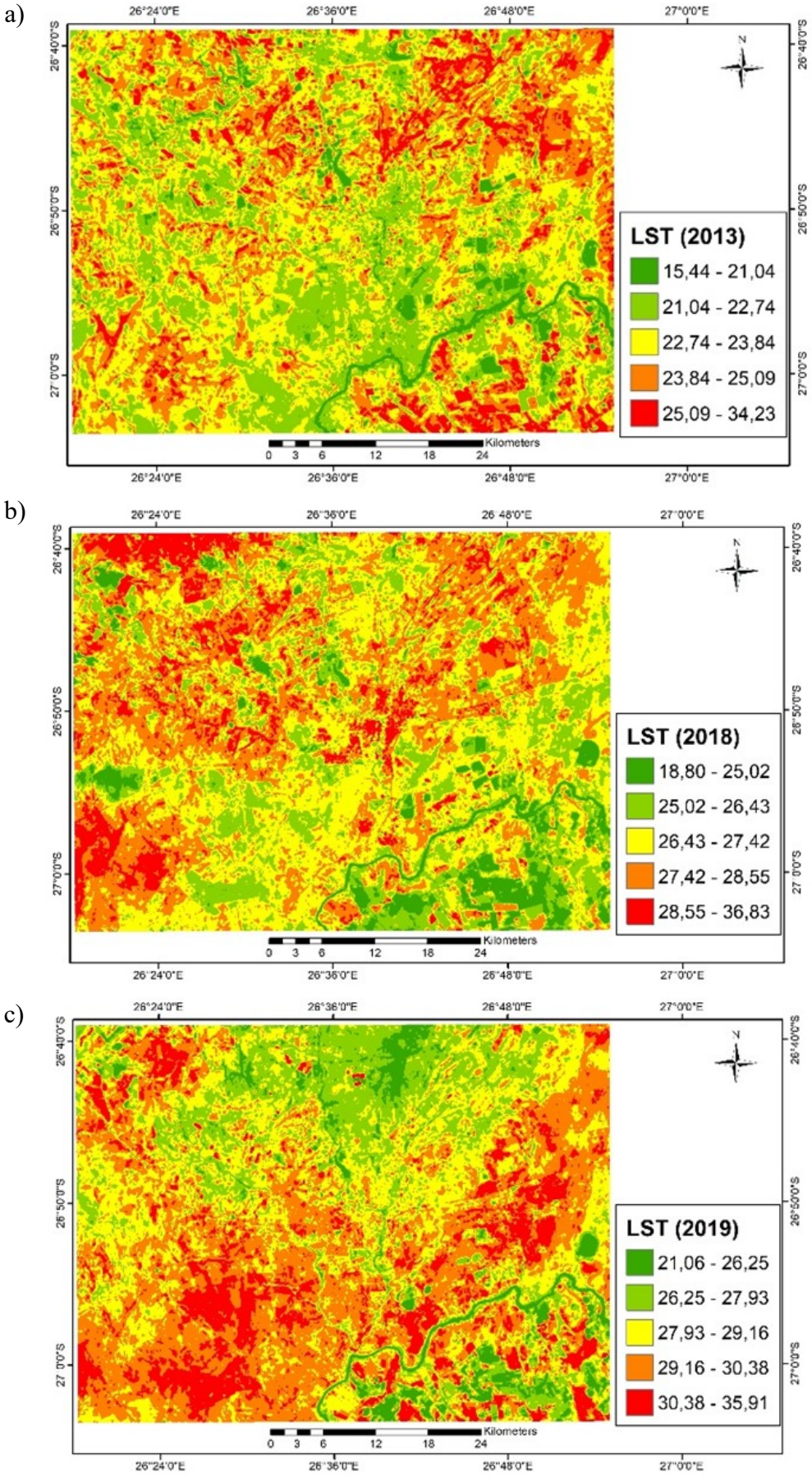

Fig. 7. Spatial-temporal pattern of LST dynamics of KOSH during the summer season of the year (a) 2013, (b) 2018 and (c) 2019

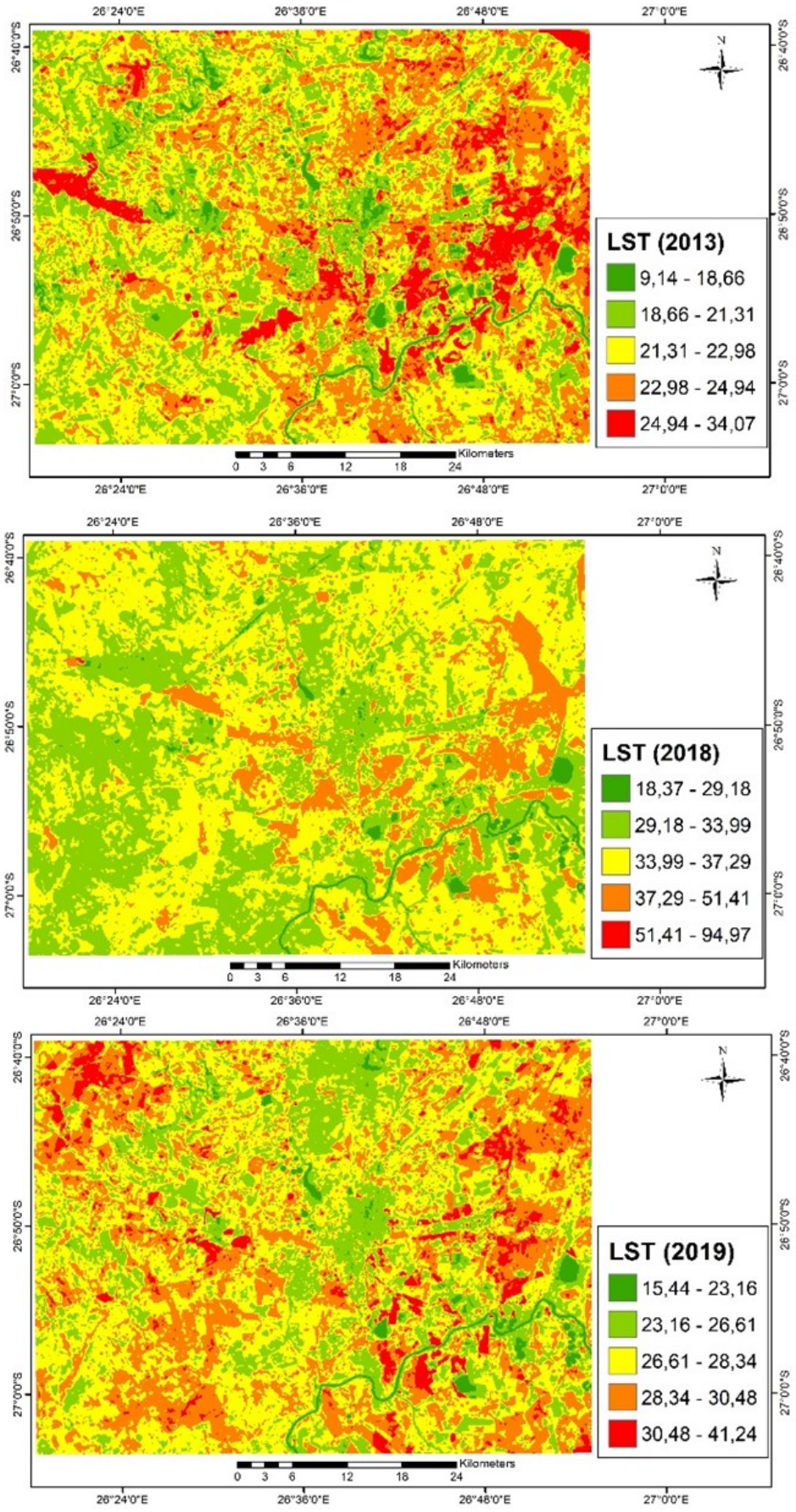

Fig. 8. Spatial-temporal pattern of LST dynamics of KOSH during the spring season of the year (a) 2013, (b) 2018 and (c) 2019

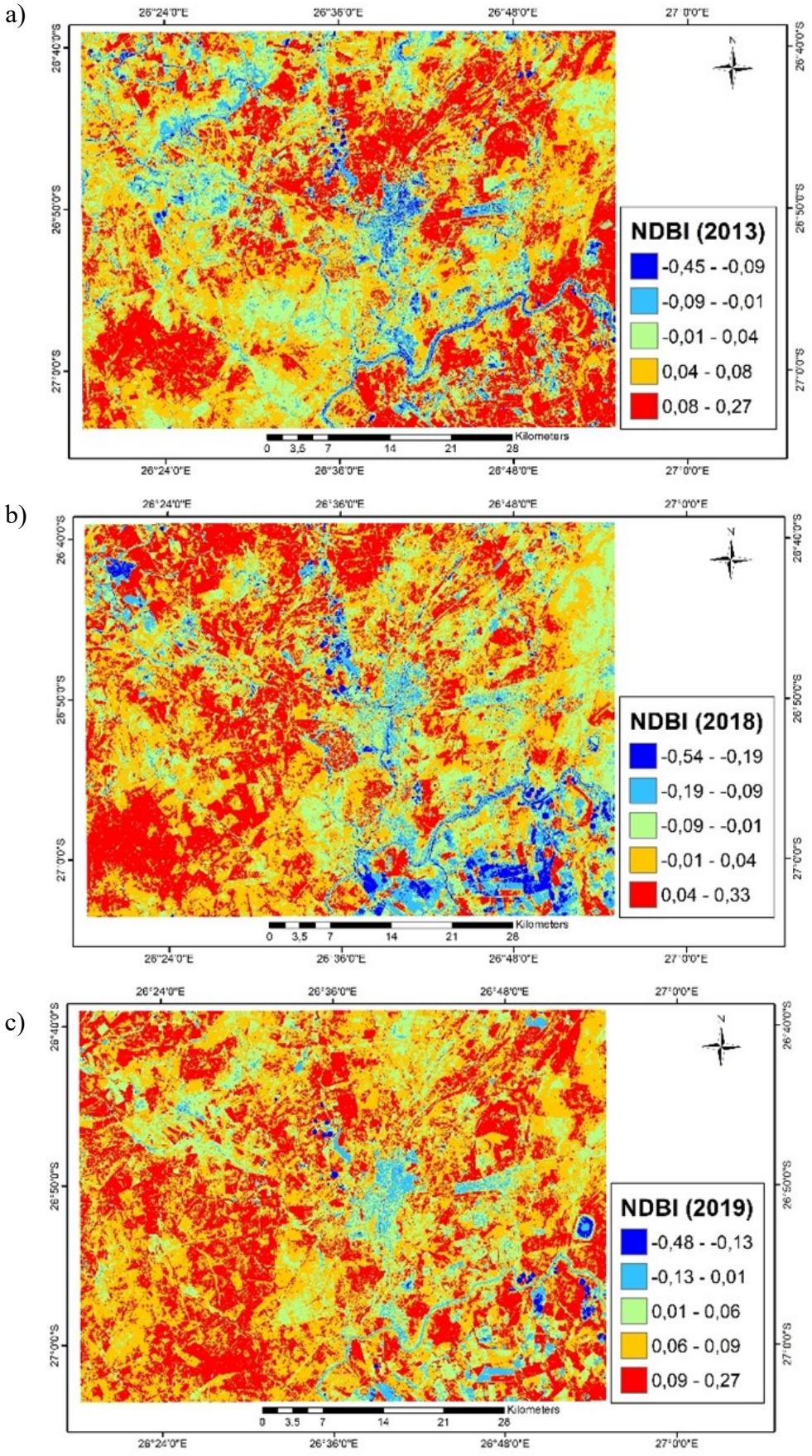

Fig. 9. Spatial-temporal pattern of NDBI dynamics of KOSH during the summer season of the year (a) 2013, (b) 2018, (c) 2019

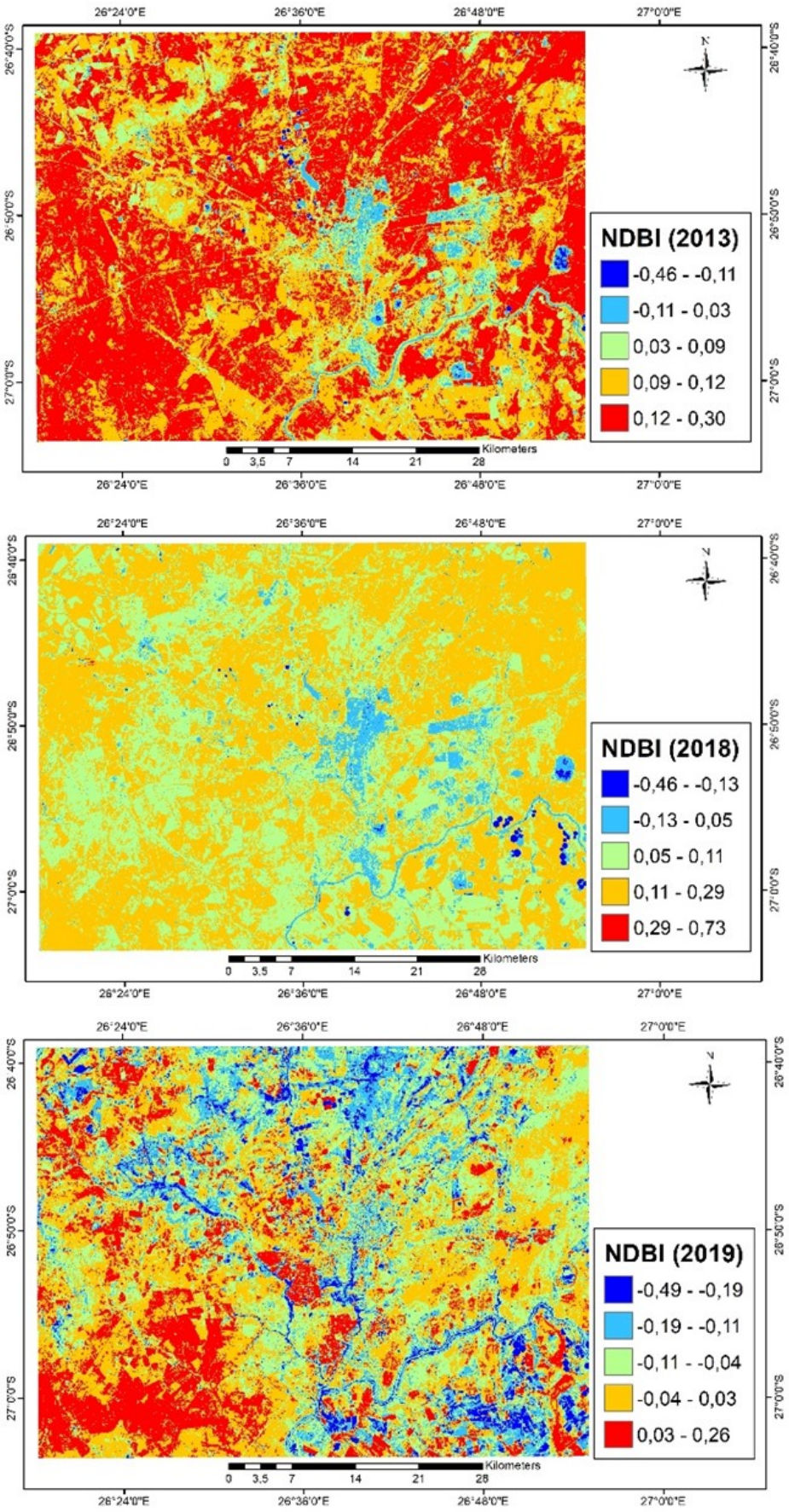

Fig. 10. Spatial-temporal pattern of NDBI dynamics of KOSH during the spring season of the year (a) 2013, (b) 2018 and (c) 2019

Table 6

Statistical summary of NDBI values in KOSH and its surrounding (2013, 2018 and 2020)

Year	Mean	Max	Min	STD
2013 Summer	0.05	0.27	-0.45	0.05
2013 Spring	0.11	0.30	-0.46	0.04
2018 Summer	-0.00	0.33	-0.54	0.08
2018 Spring	0.11	0.73	-0.46	0.04
2019 Summer	-0.04	0.26	-0.49	0.08
2019 Spring	0.08	0.27	-0.48	0.04

Drought indices monitoring

The spatial-temporal pattern of vegetation supply water index (VWSI)

VWSI can reflect the state of water supply for vegetation; but due to the great difference in the value ranges of NDVI and LST, very small values of VWSI were generated. VWSI values of the years 2013, 2018, and 2019 show most areas have experienced moderate to severe drought during the summer season. Whereas in spring seasons of these years, there is a less extreme severe drought in the area. Figure 11 shows more areas experience severe to moderate drought in all three years in a similar pattern in the summer season. The areas with extreme drought in the area are mostly the bare soil area, for example in mine tailing dumps in the area. The grassland regions are the major or mainland cover with severe drought impact. Figure 12 shows most of the areas experienced moderate drought with some parts having a severe drought. Most of KOSH shows a dominant mild to no drought condition in figure 12 and figure 11 shows areas with severe drought with moderate and no drought areas.

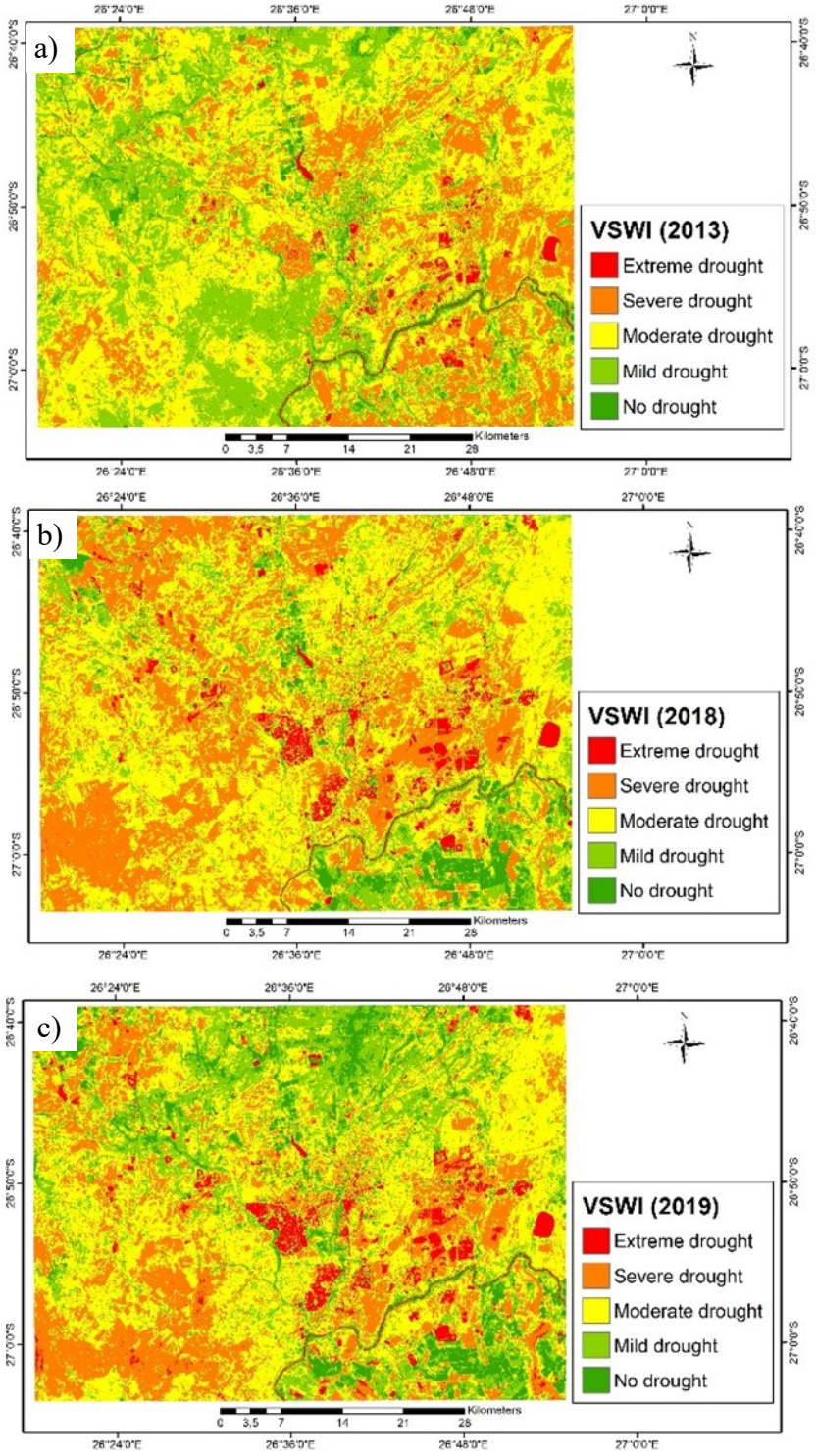

Fig. 11. Spatial-temporal pattern of VSWI dynamics of KOSH during the summer season of the year (a) 2013, (b) 2018 and (c) 2019

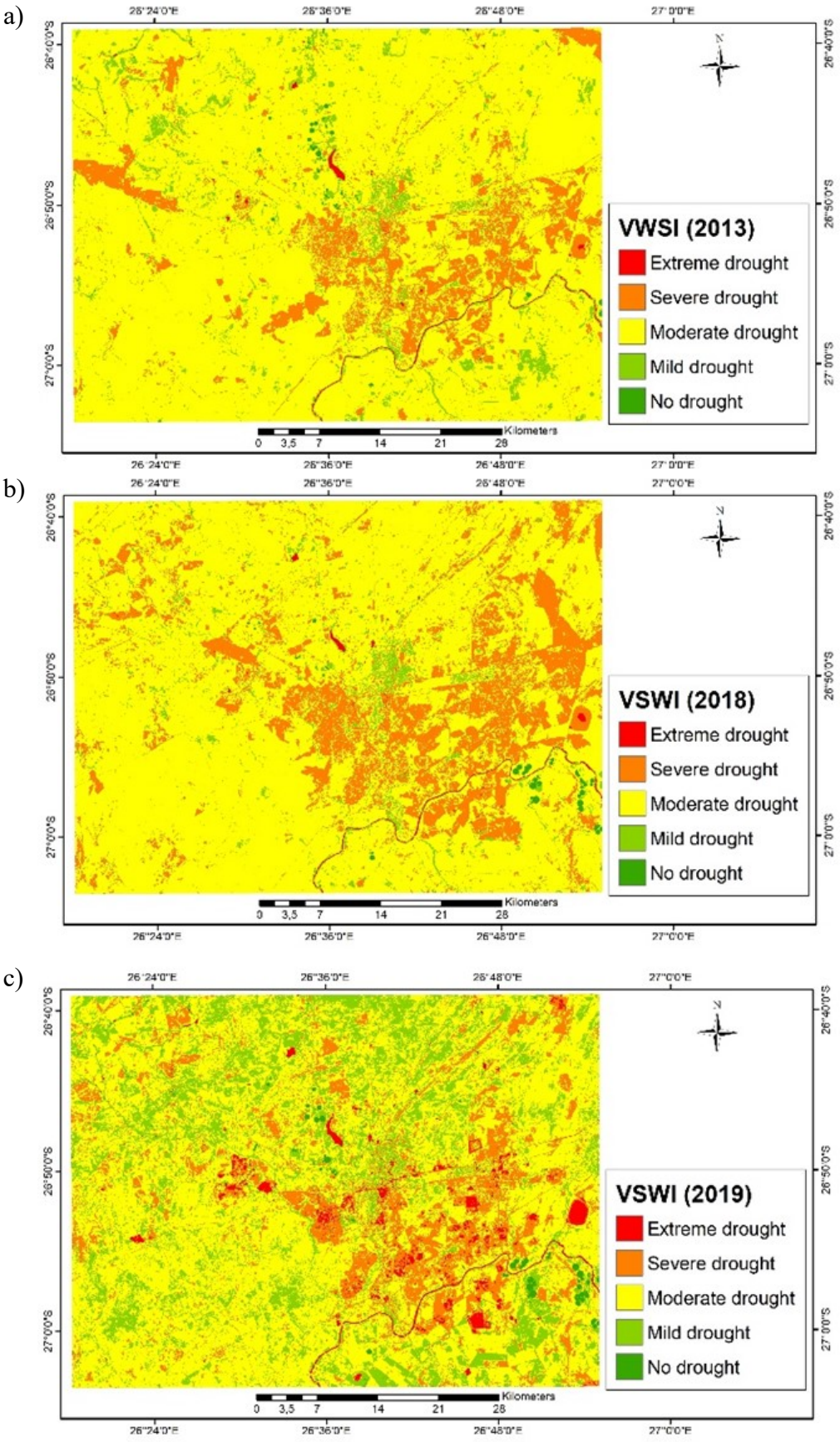

Fig. 12. Spatial-temporal pattern of VSWI dynamics of KOSH during the spring season of the year (a) 2013, (b) 2018 and (c) 2019

The spatial-temporal pattern of crop water supply index (CWSI)

Crop water supply algorithm show results of the spread of drought-affected land cover-open class land. CWSI method for all three years showed locations with water stress (fig. 13). CWSI is very different due to the appearance of undeveloped land which has a dominant value of high surface temperatures. CWSI is more relevant to the condition of having low soil moisture which proved that in many areas there is not much water on the surface. Figure 14 shows spring season results were in the year 2018 the results shows differs than the year 2013 and 2019.

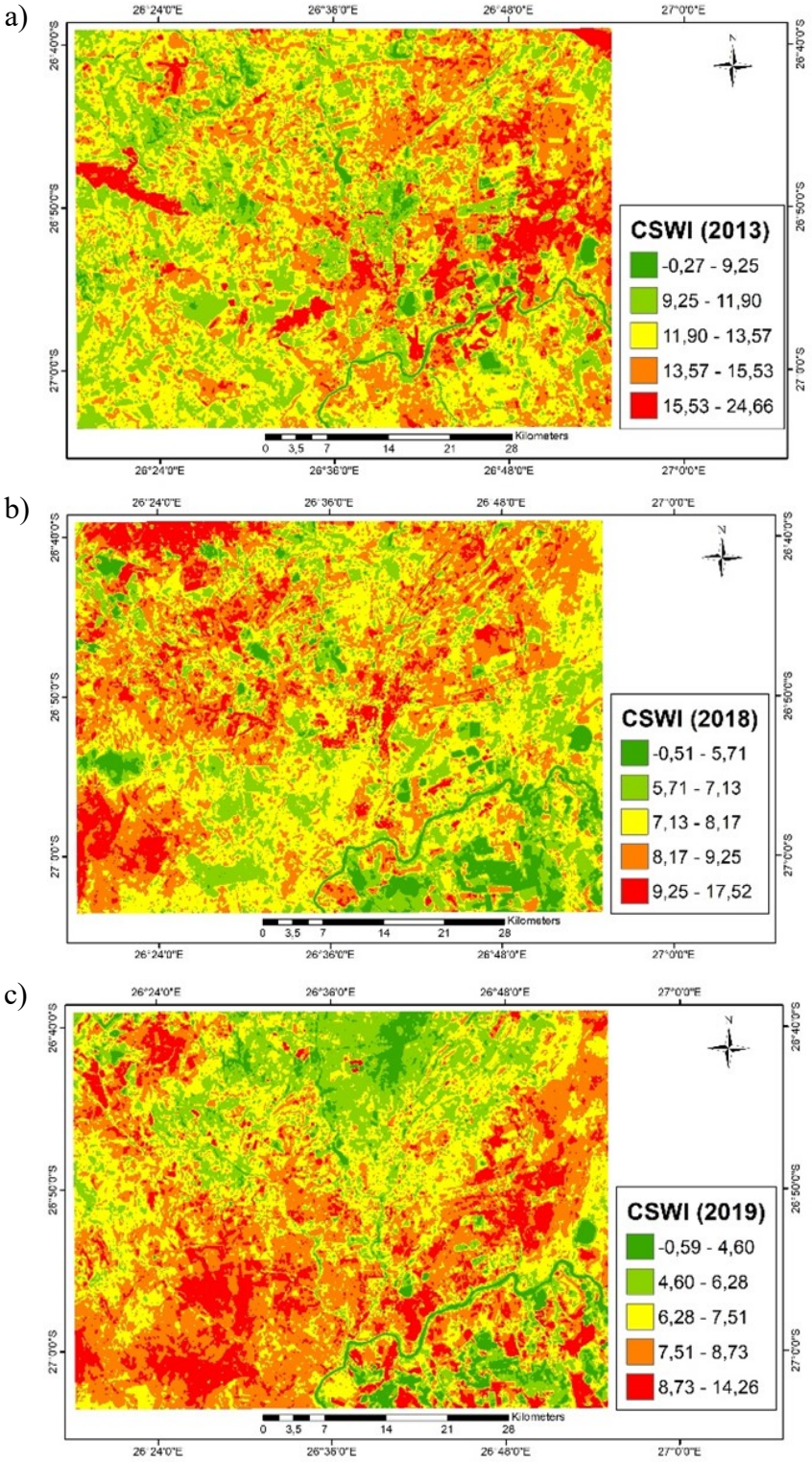

Fig. 13. Spatial-temporal pattern of CSWI dynamics of KOSH in the summer season of the year (a) 2013, (b) 2018 and (c) 2019

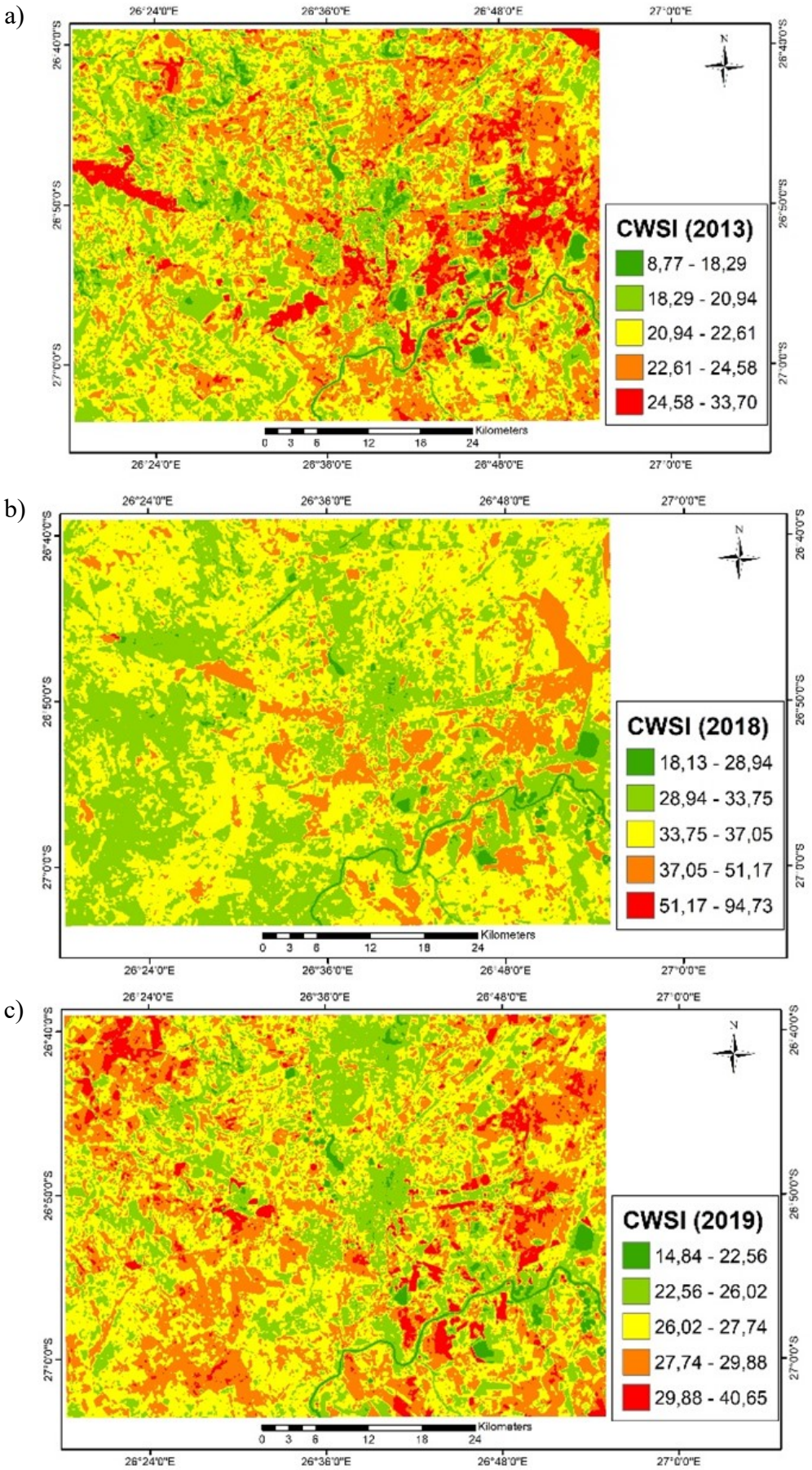

Fig. 14. Spatial-temporal pattern of CSWI dynamics of KOSH during the spring season of the year (a) 2013, (b) 2018 and (c) 2019

The spatial-temporal pattern of temperature condition index (TCI)

The results of TCI and CWSI methods in the year 2013 help to detect similar areas where there is drought. Figure 15 and figure 16 show the result of TCI for the summer season of the year 2019 and spring season of the year 2018.

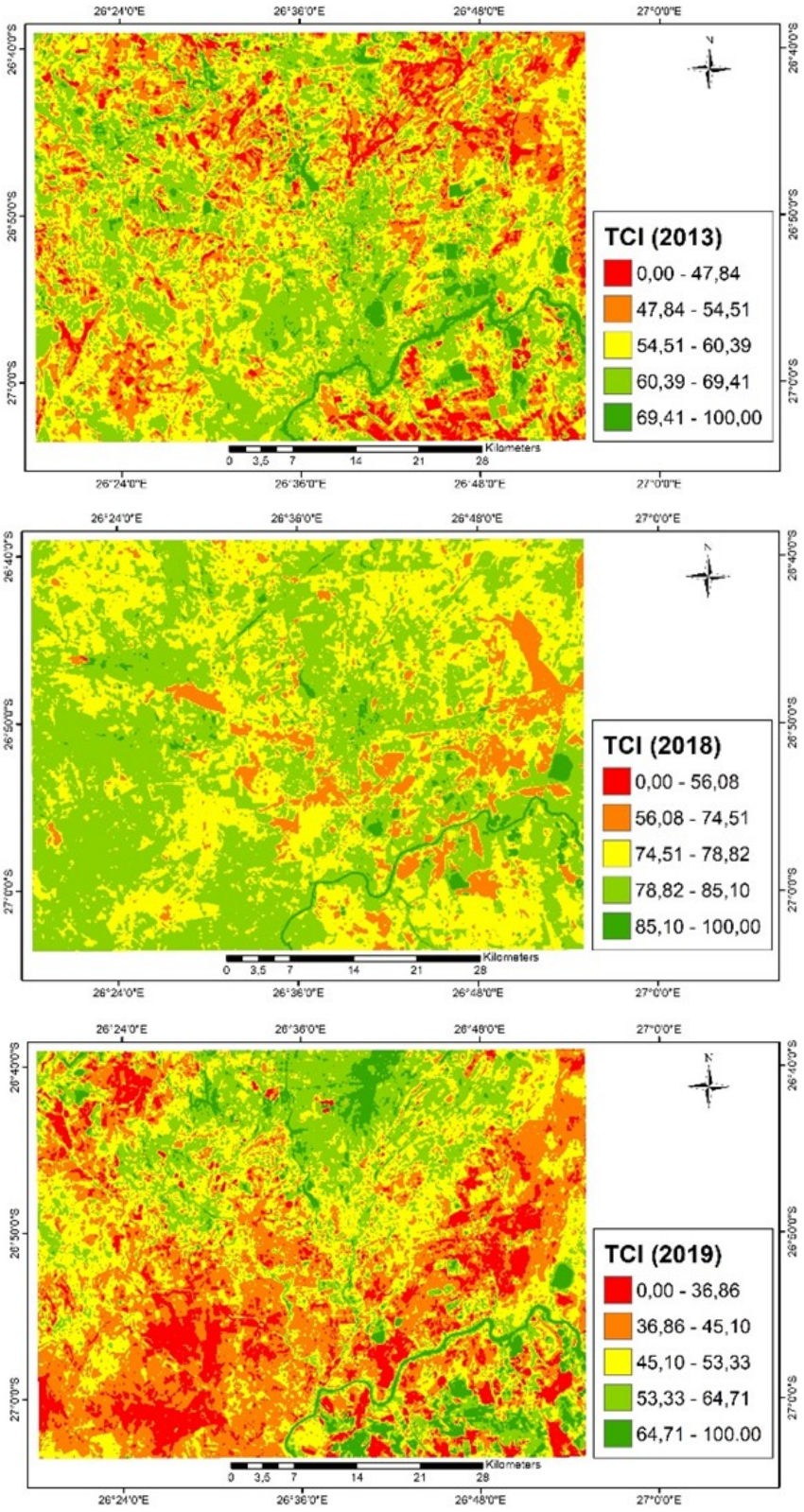

Fig. 15. Spatial-temporal pattern of TCI dynamics of KOSH during the summer season of the year (a) 2013, (b) year 2018 and (c) year 2019

From the TCI results, it can be seen that the dominant value of high surface temperatures seen in the years 2018 and 2019 matches with areas of high drought. In the year 2019, the appearance of TCI and CWSI is very different due to the appearance of undeveloped land which has a dominant value of high surface temperatures. TCI in 2019 is still able to distinguish the wet location. In all three images in the summer seasons of the study period, more areas that are experiencing drought can be detected (fig. 16).

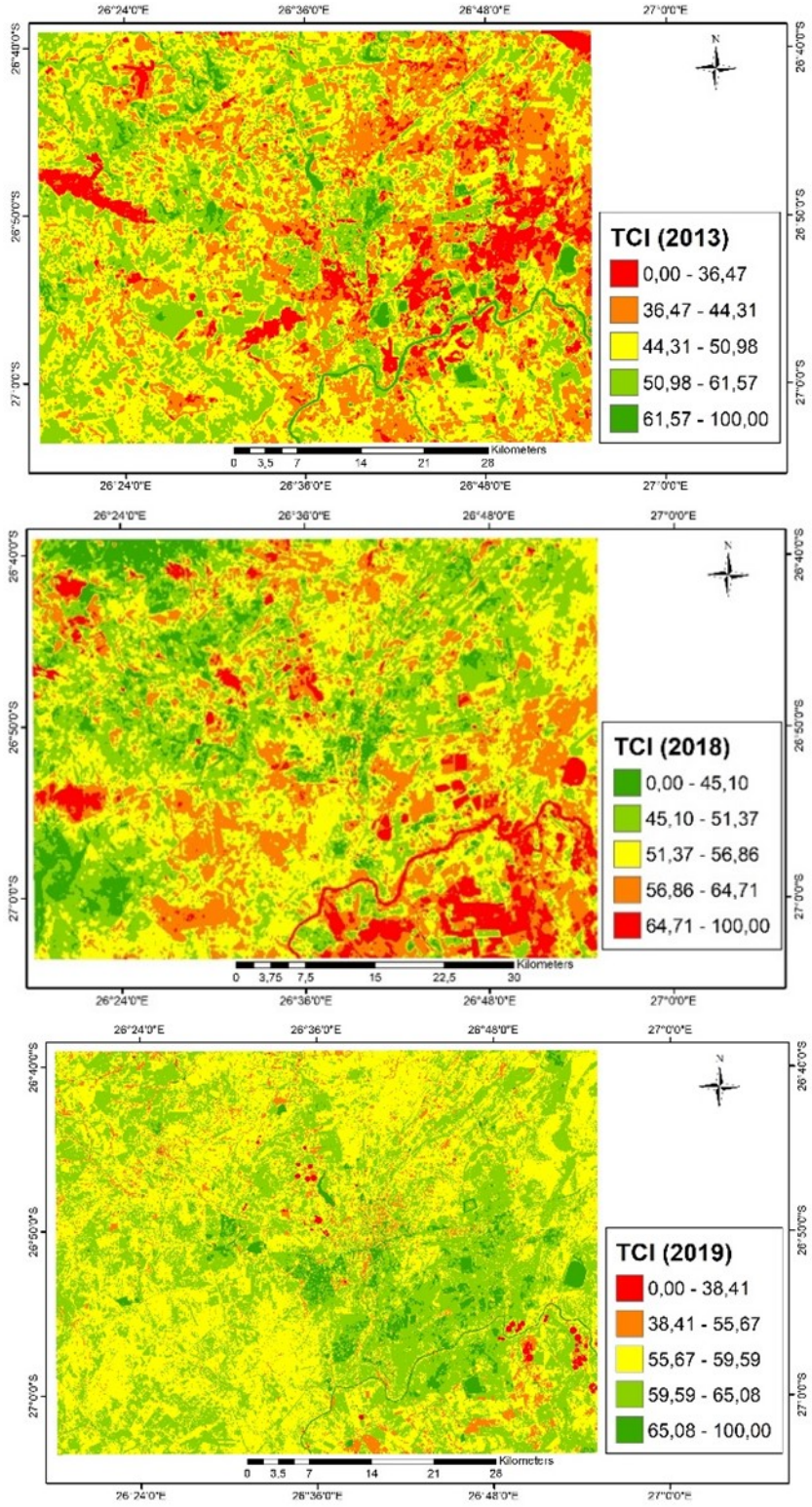

Fig. 16. Spatial-temporal pattern of TCI dynamics of KOSH during the spring season of the year (a) 2013, (b) 2018 and (c) 2019

Conclusion

The presented study could successfully estimate land surface temperature (LST) and drought indices and analyse the changing pattern of the LST and other indices. The results show that high surface temperature values have a positive correlation with drought events in an area; the higher the surface temperature the higher the drought and a negative correlation with wet conditions. The drought indices VSIW, TCI and CWSI methods were tested for drought monitoring. The results also show that the LST helps to determine areas with drought without making use of drought indices. Grassland that covers most of the area in the study area experience more drought than other land covers. The finding shows areas where there is grassland cover, the LST values are high; whereas the cultivated area shows low values of LST. The findings show that LST has a negative relationship with NDVI and positive relationship with NDBI. The study also indicates mean variation between NDBI, NDVI and LST. The mean of the LST increases from 2013 – 2019 on both seasons. The results also verified that some areas have experienced drought mostly in areas with grassland cover. Most areas of the KOSH had low NDVI because of low vegetation cover. The VSWI, TCI and CSWI show results of the spread of drought across the area where some areas experience severe drought. The results indicate that LST in certain parts of the area especially to the southwest, northwest and northeast regions experience high LST values. It is recommended that LULC mapping should also be conducted for particular periods of study to understand the dynamics of land surface temperature fluctuation concerning a specified period.

The study has shown the importance of land use/land cover in estimating the land surface temperature. An inverse (negative) relationship between LST and water bodies and vegetation cover was found while a direct positive relationship between LST and built up, and barren land area was observed. It was concluded that the increase in vegetation and water bodies can greatly decrease the land surface temperature of any region. The relationship between the LST and VI are negative which implies that the lower the LST the higher the NDVI and the higher the LST the lower the NDVI. Vegetation plays the biggest role in reducing the land surface temperature from increasing whereas on the other hand built-up area plays a major role in increasing land surface temperature. Therefore, a better option to have lower LST is to reduce the built-up land when the population is growing; rather increase in vegetation cover in the built-up area can reduce the LST.

The authors would like to register their sincere thanks to the Council for Geoscience for various resources provided for this study and the National Research Foundation of South Africa for the grant provided to undertake this study. The USGS is also hereby thanked for providing free access to the Landsat 8 data used in this study.

References

1. Balew, A.; Korme, T. Monitoring land surface temperature in Bahir Dar city and its surrounding using Landsat images. *Egyptian Journal of Remote Sensing and Space Science*. 2020. https://doi.org/10.1016/j.ejrs.2020.02.001
2. Brohan, P; Kennedy, J.J.; Harris, I.; Tett, S.F; Jones, P.D. Uncertainty estimates in regional and global observed temperature changes: a new data set from 1850. *Journal of Geophysical Research*: *Atmospheres*, **2006**, *111*, D12106. http://dx.doi.org/10.1029/2005JD006548
3. Cammalleri, C.; Vogt, J. On the Role of Land Surface Temperature as Proxy of Soil Moisture Status for Drought Monitoring in Europe. *Remote Sensing*, **2015**, *7*, 16849–16864.
4. Chastain, R., Housman, I., Goldstein, J.; Finco, M. Empirical cross sensor comparison of Sentinel-2A and 2B MSI, Landsat-8 OLI, and Landsat-7 ETM+ top of atmosphere spectral characteristics over the conterminous United States. *Remote Sensing of Environment*, **2019**, *221*, 274–285.
5. Chen, F.; Yang, S.; Yin, K.; Chan, P. Challenges to quantitative applications of Landsat observations for the urban thermal environment. *Journal of Environmental Sciences*, **2017**, *59*, 80–88.
6. Duan, S.B.; Li, Z.L.; Tang, B.H.; Wu, H.; Tang, R.. Generation of a time-consistent land surface temperature product from MODIS data. *Remote Sensing of Environment*, **2014**, *140*, 339–349.
7. Faris, A.A; Reddy, Y.S. Estimation of urban heat island using Landsat ETM+ imagery at Chennai city—a case study. *International Journal of Earth Sciences and Engineering*, 2010, 3, 332–340.

8. He, J.; Zhao, W.; Li, A.; Wen, F.; Yu, D. The impact of the terrain effect on land surface temperature variation based on Landsat-8 observations in mountainous areas. *International Journal of Remote Sensing*, **2019**, *40*, 1808–1827.
9. Herrero-Huerta, M.; Lagüela, S.; Alfieri, S.M.; Menenti, M. Generating high-temporal and spatial resolution TIR image data. *International Journal of Applied Earth Observation and Geoinformation,* **2019**, *78*, 149–162.
10. Hansen, J.; Ruedy, R.; Sato, M.; Lo, K. Global surface temperature change. *Reviews of Geophysics*, **2010**, *48*, RG4004. https://doi.org/10.1029/2010RG000345
11. Jin, M., Li, J., Wang, C. and Shang, R. 2015. A practical split-window algorithm for retrieving land surface temperature from Landsat-8 data and a case study of an urban area in China. Remote Sensing, 7, 4371–4390.
12. Kogan, F.N. 1998. Global drought and flood-watch from NOAA polar-orbitting satellites. Advances in Space Research, 21, 477–480.
13. Kothe, E.J., Ling, M., North, M., Klas, A., Mullan, B.A. and Novoradovskaya, L. 2019. Protection motivation theory and pro-environmental behaviour: A systematic mapping review. In: Australian Journal of Psychology. Wiley-Blackwell Publishing Ltd, 411–432.
14. Landsat 8 Data Users Handbook. Available at https://www.usgs.gov/core-science-systems/nli/landsat/landsat-8-data-users-handbook (accessed 11 September 2020).
15. Ngie, A., Abutaleb, K., Ahmed, F., Taiwo, O.J., Darwish, A.A. and Ahmed, M. 2017. Estimation of land surface temperatures from landsat ETM+ images for Durban, South Africa. Rwanda Journal, 1.
16. Owojori, A. and Xie, H. 2005. Landsta image-based LULC changes of San Antonio, Texas using advance atmospheric correction and object-orientated image analysis approaches. Remote sensing image processing and analysis (ES 6973).
17. Pal, S. and Ziaul, S. 2017. Detection of land use and land cover change and land surface temperature in English Bazar urban centre. Egyptian Journal of Remote Sensing and Space Science, 20, 125–145.
18. Quintano, C., Fernández-Manso, A., Calvo, L., Marcos, E. and Valbuena, L. 2015. Land surface temperature as a potential indicator of burn severity in forest Mediterranean ecosystems. International Journal of Applied Earth Observation and Geoinformation, 36, 1–12.
19. Rehman, Z., Kazmi, S., Khanum, F. and Samoon, Z. 2015. Analysis of Land Surface Temperature and NDVI Using Geo-Spatial Technique: A Case Study of Keti Bunder, Sindh, Pakistan. Journal of Basic & Applied Sciences, 11, 514–527.
20. Rosas J, Houborg R, McCabe M.F. 2017. Sensitivity of Landsat 8 surface temperature estimates to atmospheric profle data: a study using MODTRAN in dryland irrigated systems. Remote Sens 9:1–27. https://doi.org/10.3390/rs9100988
21. Simó, G., García-Santos, V., Jiménez, M., Martínez-Villagrasa, D., Picos, R., Caselles, V. and Cuxart, J. 2016. Landsat and Local Land Surface Temperatures in a Heterogeneous Terrain Compared to MODIS Values. Remote Sensing, 8, 849.
22. Sobrino, J.A., Oltra-Carrió, R., Sòria, G., Bianchi, R. and Paganini, M. 2012. Impact of spatial resolution and satellite overpass time on evaluation of the surface urban heat island effects. Remote Sensing of Environment, 117, 50–56.
23. Sobrino, J.A. and Romaguera, M. 2004. Land surface temperature retrieval from MSG1-SEVIRI data. Remote Sensing of Environment, 92, 247–254.
24. Suresh S, Ajay SV, Mani K (2016) Mountain landscape of Devikulam Taluk using Landsat 8 data. Int J Res Eng Technol 5:92–96.
25. Thomas, A. Mapping of surface deformation associated with the 5.2 magnitude Stilfontein earthquake of 3 April 2017 using radar interferometry. *Egyptian Journal of Remote Sensing and Space Science*. **2020** https://doi.org/10.1016/j.ejrs.2020.01.005
26. Torrion, J.A., Maas, S.J., Guo, W., Bordovsky, J.P. and Cranmer, A.M. 2014. A three-dimensional index for characterizing crop water stress. Remote Sensing, 6, 4025–4042.
27. Ustin, S.L., Roberts, D.A., Gamon, J.A., Asner, G.P. and Green, R.O. 2004. Using imaging spectroscopy to study ecosystem processes and properties. BioScience, 54, 523–534.
28. Weng, Q., Lu, D. and Schubring, J. 2004. Estimation of land surface temperature-vegetation abundance relationship for urban heat island studies. Remote Sensing of Environment, 89, 467–483.
29. Xiao, R. bo, Ouyang, Z. yun, Zheng, H., LI, W. feng, Schienke, E.W. and Wang, X. ke 2007a. Spatial pattern of impervious surfaces and their impacts on land surface temperature in Beijing, China. Journal of Environmental Sciences, 19, 250–256.
30. Xiao, R. bo, OUYANG, Z. yun, zheng, H., LI, W. feng, Schienke, E.W. and Wang, X. ke 2007b. Spatial pattern of impervious surfaces and their impacts on land surface temperature in Beijing, China. Journal of Environmental Sciences, 19, 250–256.
31. Yang, L., Cao, Y.G., Zhu, X.H., Zeng, S.H., Yang, G.J., He, J.Y. and Yang, X.C. 2014. Land surface temperature retrieval for arid regions based on Landsat-8 TIRS data: A case study in Shihezi, Northwest China. Journal of Arid Land, 6, 704–716.